Lecture 2: Microlensing in Lensed QSOs
Case study: SDSSJ1004+4112, SDSSJ1029+2623, HE1104-1805

Emilio E. Falco
Smithsonian Astrophysical Observatory
F. L. Whipple Observatory
670 Mt. Hopkins Rd.
Amado, AZ 85645, USA

Inspiration:

"Measuring Microlensing using Spectra of Multiply Lensed QSOs"
V. Motta et al. 2012 ApJ 755, 1, 82 (VM12)

1. LENSING BY SUBSTRUCTURES

Lenses are very apt tools to study the structure of QSOs and of the lens galaxies (Schneider et al. 1992; Kochanek 2004; Wambsganss 2006). Simple lens models reproduce the positions of lensed QSO images, but often fail to account for the optical flux ratios of these images. Lensing by "substructures" causes these anomalies in lens galaxies (Dalal & Kochanek 2002; Keeton 2002; Bradac et al. 2002; Metcalf & Zao 2002; Moustakas & Metcalf 2003). The substructures are either dark matter subhalos or stars; their effects are millilensing and microlensing, respectively. We will only look at microlensing.

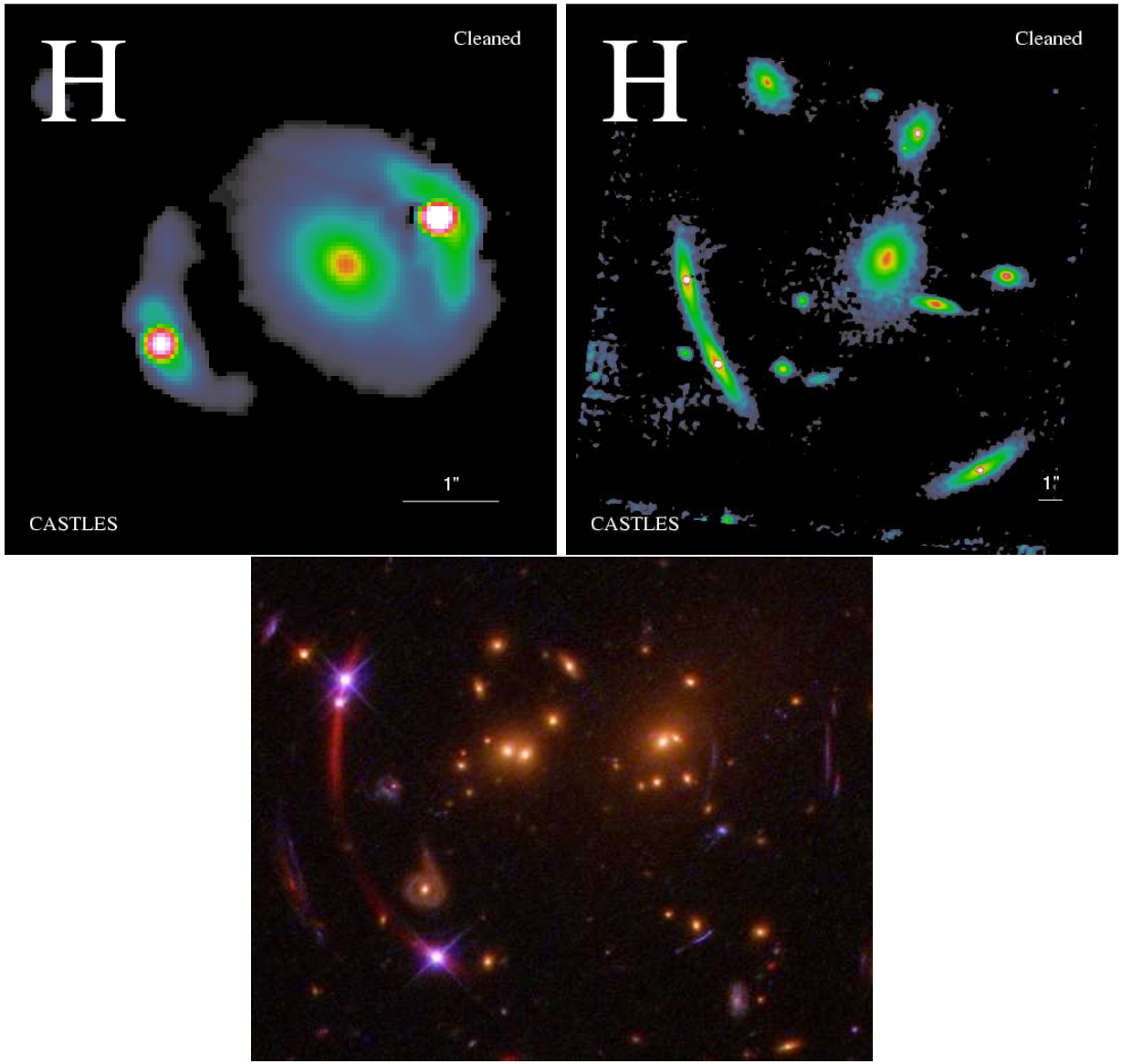

Fig. 1.— A subset of targets for measuring microlensing in VM12: CASTLES H-band images of HE1104 and SDSS1004. ACS RGB composite of SDSS1029 (Oguri et al. 2012).

A substructure causes a flux-ratio anomaly only if its Einstein ring is large compared to the emitting region.

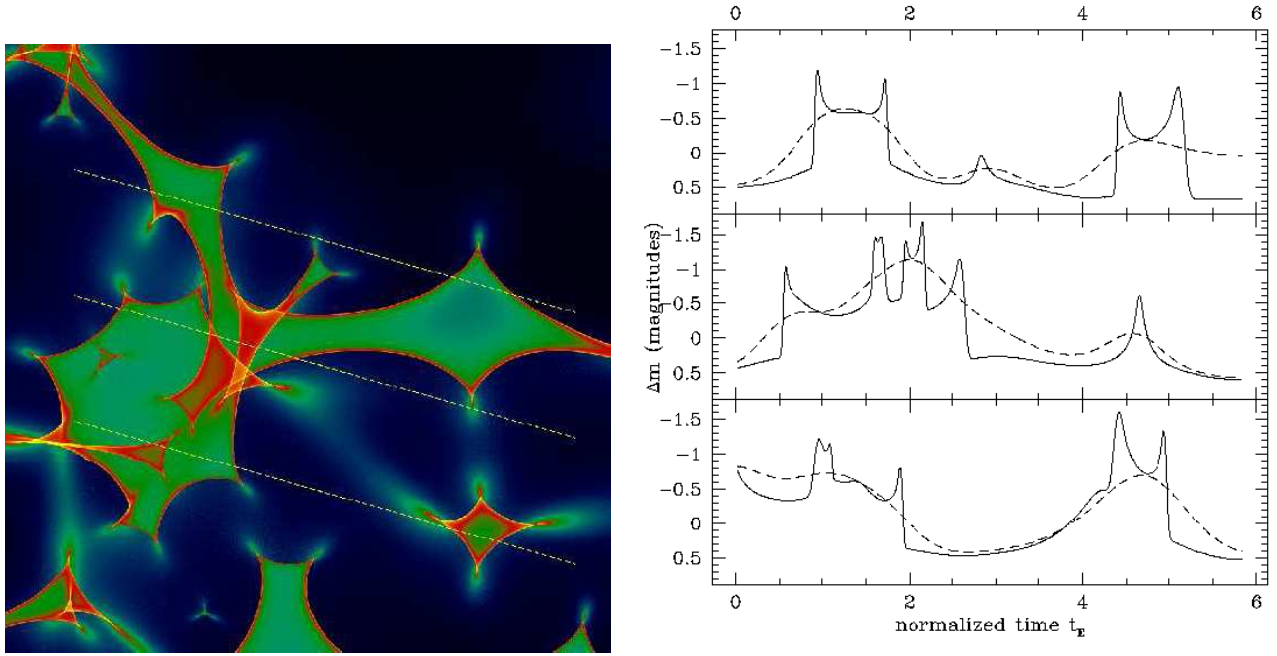

Fig. 2.— From (Wambsganss 2006). Left: microlensing magnification pattern produced by stars in a lens galaxy. Blue to red colors mean increasing magnifications. Sharp caustics correspond to the largest magnifications. The 3 dashed lines are tracks for a background quasar. Right: microlensing lightcurves for the tracks at left. The solid (dashed) line is for a Gaussian source with a width about 3% (30%) of the Einstein radius.

Table 1. Selected Image Properties

Lens Name	z_L	z_S	Max. separation
SDSS1004+4112	0.68	1.734	$16\farcs0$
SDSS1029+2623	0.55	2.197	$22\farcs5$
HE1104-1805	0.73	2.32	$3\farcs2$

Table 2. Log of observations for the subset

Objects	Pair[a]	Δ[b] ($''$)	Instrument	Grating	Date	Airmass	P.A.[c]	Seeing[d]	Exposure[e]
SDSS1004+4112	AB	3.8	MMT/Blue-Channel	300	2008/01/12	1.028	200.40	0.61	2×900
SDSS1029+2623	AB	22.6	MMT/Blue-Channel	300	2008/01/11	1.072	11.12	0.67	1800
HE1104-1805	AB	3.2	MMT/Blue-Channel	300	2008/01/11	1.766	114.66	0.67	1000
	AB	3.2	VLT/FORS2	300V	2008/04/07	1.315	64.18	0.60	3×250

[a]Target images

[b]Separation, observed images in arcsec

[c]degrees E of N

[d]arcsec

[e]Seconds

Because the sizes of QSO continuum regions depend on the emission wavelengths, microlensing by stars in a lens galaxy results in a wavelength-dependent magnification of the continuum (Mosquera, Muñoz & Mediavilla 2009; Mediavilla et al. 2011) that may be strong in the UV and optical but negligible in the IR. Microlensing could also affect the high ionization broad emission lines (BEL) that arise from the inner part of the broad-line region (BLR). It affects the broad wings of the profiles of the high ionization lines of high velocity emitters, leaving unchanged the cores (Richards et al. 2004; Lewis & Ibata 2004; Gómez-Álvarez et al. 2006). Low ionization BEL and narrow emission lines (NEL) come from considerably larger regions and should be insensitive to microlensing (Abajas et al. 2002).

Finding microlensing in strongly-lensed QSOs requires monitoring over long periods, up to several years. There have been a number of successes (a striking one being Q2237+030):

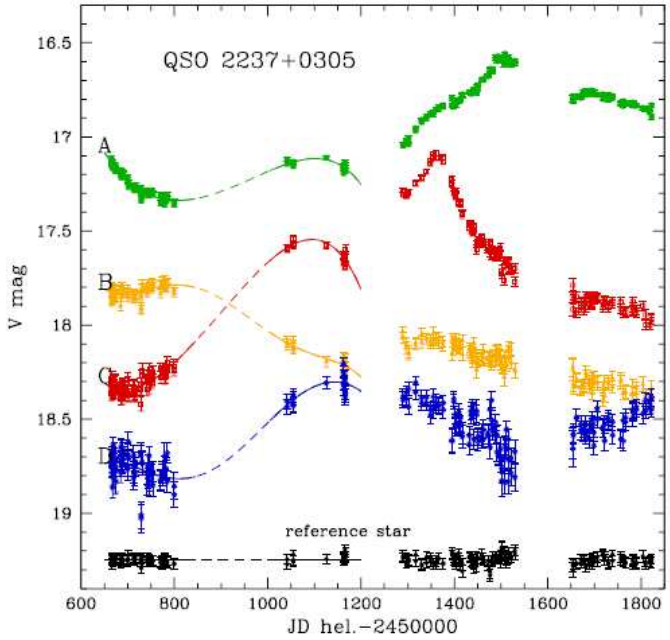

Fig. 3.— From (Wambsganss 2006). Lightcurves covering nearly 3 years of fluctuations of the 4 lensed images of the quasar Q2237+0305, with amplitudes of over 1 mag. Measured by OGLE (Wozniak et al. 2000, ApJ 529, 88).

Microlensing searches using optical imaging concentrate on quadruples: the effect of substructure is more apparent at high magnification (Witt et al. 1995; Schechter & Wambsganss 2002; Pooley et al. 2007). Quadruples provide enough constraints to fit the simplest singular isothermal (SIS) model (Schechter & Wambsganss 2002; Kochanek & Dalal 2004) and find any flux anomalies. Double lenses provide fewer constraints on models unless the fluxes are used as additional constraints. In these cases, the flux ratios of emission lines (Wisotzki et al. 1993; Mediavilla et al. 2009, 2011) or in the IR (Agol et al. 2007) have been used, assuming that the emission regions are larger than the microlensing source and dust extinction is negligible Mediavilla et al. (2011).

2. GOALS

- Avoid the burdens and limitations of monitoring and broad-band photometry of images, with single-epoch spectroscopy.
- Use flux ratios for the cores of emission lines in image pairs to set a no-microlensing baseline.
- Find microlensing magnification from the offset of the continuum flux ratios relative to the no-microlensing baseline.
- Estimate the variation of microlensing as a function of wavelength, known as chromatic microlensing. Lensing itself is achromatic, but source sizes vary with wavelength and induce chromatic variations.
- Equipped with chromatic microlensing, constrain the sizes of accretion disks of lensed QSOs.

3. VM12 METHODS

To detect microlensing using spectra of lensed QSOs one needs:

1. Excellent seeing conditions ($\leq 0.8''$).
2. Spectra with high SNRs ($SNR \simeq 40$).
3. Spectra with sufficient spectral resolution ($v_{res} < 200$ km/s) to resolve the shape of the line profiles.
4. Simultaneous, spatially-separated spectra of pairs of lensed QSO images to compare their continuum and emission lines at different wavelengths.

The data in VM12 satisfy these prescriptions (Table 2). They reduced their data with standard IRAF tasks: bias subtraction, flat fielding, extraction of 1-D spectra, wavelength calibration, and cosmic-ray rejection when multiple exposures were available. As they were only interested in flux ratios (i.e. magnitude difference $m_B - m_A = -2.5 \log(F_B/F_A)$), they did not flux-calibrate their data.

3.1. SYSTEMATIC ERRORS

- Spectrum cross-contamination: There was essentially no cross-contamination between the spectra of lensed QSO image pairs in the VM12 sample, because they selected pairs with much larger separations than the typical seeing ($\leq 0\farcs7$). They estimated that cross-contamination was negligible.

- Long-slit losses: VM12 aligned the slit at the position angle (PA) defined by each pair of images. A small amount of the blue part of each spectrum was lost because they didn't align the slit with the parallactic angle. Given the airmass ranges of the observations and the atmospheric conditions at each observatory, the relative losses were $< 1\%$ in all MMT spectra; for the VLT spectra, the losses were $< 9\%$ due to an error in the PA of the observations. Because of the small (in this context) separation between pairs of images ($2\farcs6$ to $22\farcs6$), the losses were nearly identical for both spectra in each case. As the goal was to measure flux ratio changes with wavelength, those losses did not affect the VM12 results.

3.2. MEASUREMENT OF MICROLENSING IN THE CONTINUUM

To separate microlensing and extinction, VM12 measured the offsets between continuum and emission line flux ratios (Motta et al. 2002; Wucknitz et al. 2003; Wisotzki et al. 2003; Mediavilla et al. 2009, 2011; Sluse et al. 2011). The method succeeds because QSO emission lines have multiple components that are radiated from a wide range of distances from the central continuum source. This allows the separation into components affected by microlensing and extinction from those that are unaffected.

The low ionization lines (LIL) and the cores of the high ionization lines (HIL) are dominated by a component (FWHM $\sim 600 - 5000\,\mathrm{km\,s^{-1}}$) radiated from a large region that is insensitive to microlensing by solar-mass objects (Marziani et al. (2010)). However, the broad wings of the emission lines (FWHM $\sim 10000\,\mathrm{km\,s^{-1}}$), emerge from the inner parts of the BLR and may be microlensed. VM12 used only the line cores (dominated by the narrow-line region and the outer regions of the BLR) as the reference to set the baseline for no microlensing. To compute the core flux components (Marziani et al. 2010), they used a simple narrow-band decomposition as in Sluse et al. (2011). The core flux is the continuum-subtracted flux integrated in a narrow velocity interval (from 25 to 90 Å, depending on the line profile shapes for the different sources) centered on the peak of each line.

To estimate the continuum near and under each emission line, VM12 fitted a straight line, $y_c = a\lambda + b$, to the continuum on either side of the emission line, given a total wavelength range (λ_A, λ_B). The flux in the continuum is the integral below the fitted function y_c, i.e. $F_c = (a/2)(\lambda_B - \lambda_A)^2 + b(\lambda_B - \lambda_A)$. The error is $\Delta F_c = (\Delta a/2)(\lambda_B - \lambda_A)^2 + \Delta b(\lambda_B - \lambda_A)$.

The emission-line flux is the integrated emission line profile in each continuum-subtracted emission line. VM12 separated the line core from the wings which could be affected by microlensing. The error in the narrow emission line is the error in the continuum fitting. Where the emission line was affected by absorption lines, a narrow integration window was used (10 to 15 Å in the case of SDSS1029+2623). In most cases these absorptions are weak, so they can be easily avoided. When the absorptions are broad and affect the central part of the emission lines (e.g. SDSS1029+2623) the measurements have correspondingly larger uncertainties.

3.3. ACCRETION DISKS

Where VM12 detected chromatic microlensing, they could study the structure of the accretion disk in the lensed QSO by estimating its size and temperature profile. They model the accretion disk as a Gaussian, $I \propto \exp(-R^2/2r_s^2)$, with a radius that varies with wavelength, $r_s \propto \lambda^p$. To estimate the probability of reproducing the measurements VM12 randomly placed a Gaussian source on simulated microlensing magnification maps of 30×30 Einstein Radii (1000×1000 pixels) for SDSS1004+4112 and $\sim 59 \times 59$ Einstein Radii (2000×2000 pixels) for HE1104-1805 computed for each image. They used the Inverse Polygon Mapping method (Mediavilla et al. 2006).

The convergence (κ) and shear (γ) for each image came from models in the literature (see e.g. Kochanek et al. 2006; Mediavilla et al. 2009). VM12 used $\alpha = 0.1$ for the fraction of mass in compact objects, a reasonable value according to current estimates (see e.g. Schechter & Wambsganss 2002; Mediavilla et al. 2009; Pooley et al. 2009). VM12 consider 1 $M_\odot$ microlenses. Following a Bayesian approach as in Mediavilla et al. (2011), VM12 estimated the probability of r_s and p conditioned on the measured microlensing magnifications for both uniform and logarithmic priors on r_s. VM12 considered these two size priors to analyze the sensitivity of their study to such priors (see Morgan et al. 2010; Mediavilla et al. 2011). They considered a range of 1 to 15 light-days ($2.6 - 38.9 \times 10^{15}$ cm) for r_s and a range of 0 to 3 for p.

3.4. DUST EXTINCTION

When one looks at different lensed QSO images, one looks through different positions in the lens galaxy. That means different amounts of dust and gas and possible differential extinction. Falco et al. (1999) measured the mean differential extinction, $\Delta E(B-V)$, in 23 lens galaxies using HST broad-band filters. This extinction affects the continuum flux ratio and the emission-line fluxes (Motta et al. 2002; Mediavilla et al. 2005, 2009, 2011). As the cores of the emission lines are affected by neither microlensing nor intrinsic variability, measuring the emission line flux ratios at several wavelengths allows one to determine the existence of dust extinction in the system. VM12 fitted the extinction curve to the magnitude difference in emission lines for two images, e.g., 1 and 2 using the equation (Falco et al. 1999; Muñoz et al. 2004)

$$m_1(\lambda) - m_2(\lambda) = -2.5 \log\left(\frac{M_1}{M_2}\right) + (E_1 - E_2) R_V \left(\frac{\lambda}{1+z_L}\right),$$

where M_1/M_2 is the constant magnification ratio, $E_1 - E_2 = \Delta E$ is the extinction difference, and $R_V[\lambda/(1+z_L)]$ is the extinction curve in the lens rest frame. They minimized χ^2 per number of degree of freedom (χ^2_{DOF}) to obtain the fits.

VM12 obtained extinction estimates with the Cardelli, Clayton, & Mathis (1989) extinction curve of the Milky Way (i.e. they fixed the parameter $R_V = 3.1$) at the redshift of the lens galaxy.

3.5. INTRINSIC VARIABILITY

Continuum flux variations in QSOs do not affect NEL fluxes (Peterson 1993). Intrinsic continuum variability combined with the time delay for image pairs can produce a change in the flux ratios between images that is wavelength dependent, thus simulating changes in chromaticity. These changes should be avoided if possible, or at least estimated. For HE1104-1805, VM12 used data taken at two different epochs separated by the time delay to avoid the problem of intrinsic variability.

The effect of intrinsic variability (following Yonehara, Hirashita & Richter 2008) can be estimated, using the structure function from SDSS imaging data of QSOs (Vanden Berk et al. 2004; Ivezić et al. 2004). Take the least favorable case: an intrinsic magnitude of $M_I = -21$ for the QSO (Yonehara, Hirashita & Richter 2008), the bluest photometric band to measure variability and the two bands with the largest separation in wavelength to estimate the chromaticity variation. In the case of SDSS1004+4112 A,B with a measured time-delay of about 40 days, the expected intrinsic variability is $\lesssim 0.1$ mag and the chromaticity change is $\lesssim 0.03$ mag. For HE1104-1805 with a measured time delay of about 150 days, variability of ~ 0.1 mag and chromaticity change $\lesssim 0.05$ mag are predicted. Finally, for the largest separation system, SDSS1029+2623, variability of $\lesssim 0.2$ mag and chromaticity change of $\lesssim 0.08$ mag are expected. Changes in chromaticity from intrinsic fluctuations are expected to be small.

4. SDSS1004+4112

Inada et al. (2003) discovered the five-image lens system SDSS1004+4112 at $z_s = 1.734$. The lens is a cluster of galaxies at $z_l = 0.68$ (Oguri et al. 2004; Inada et al. 2008), which was detected in X-rays (Ota et al. 2006). The system has known CIV broad-line profile variations (Richards et al. 2004) that are argued to arise either from microlensing (Richards et al. 2004; Gómez-Álvarez et al. 2006; Abajas et al. 2007) or from small line-of-sight differences through the QSO absorbing outflows (Green 2006). Fohlmeister et al. (2008) measured a time delay of 40.6 ± 1.8 days for images A and B, and 822 ± 2 days for C and D. They estimated the microlensing amplitude was about 0.15 mag between A and B.

Compare the A and B spectra taken with the MMT: there is an enhancement in the blue wing and a decrement in the red wing of the CIV and SIV emission lines (Figure 4). Lyα and CIII] emission lines show smaller differences. The VM12 results are consistent with Richards et al. (2004); Gómez-Álvarez et al. (2006) and Lamer et al. (2006). Figure 5 shows the A and B CIV emission line profiles taken in 2004 with Keck. While the B component and the red part of the A component are the same in both epochs, the blue wing enhancement of component A is significantly smaller in 2008. This variability is the kind of change in the line profile expected from microlensing.

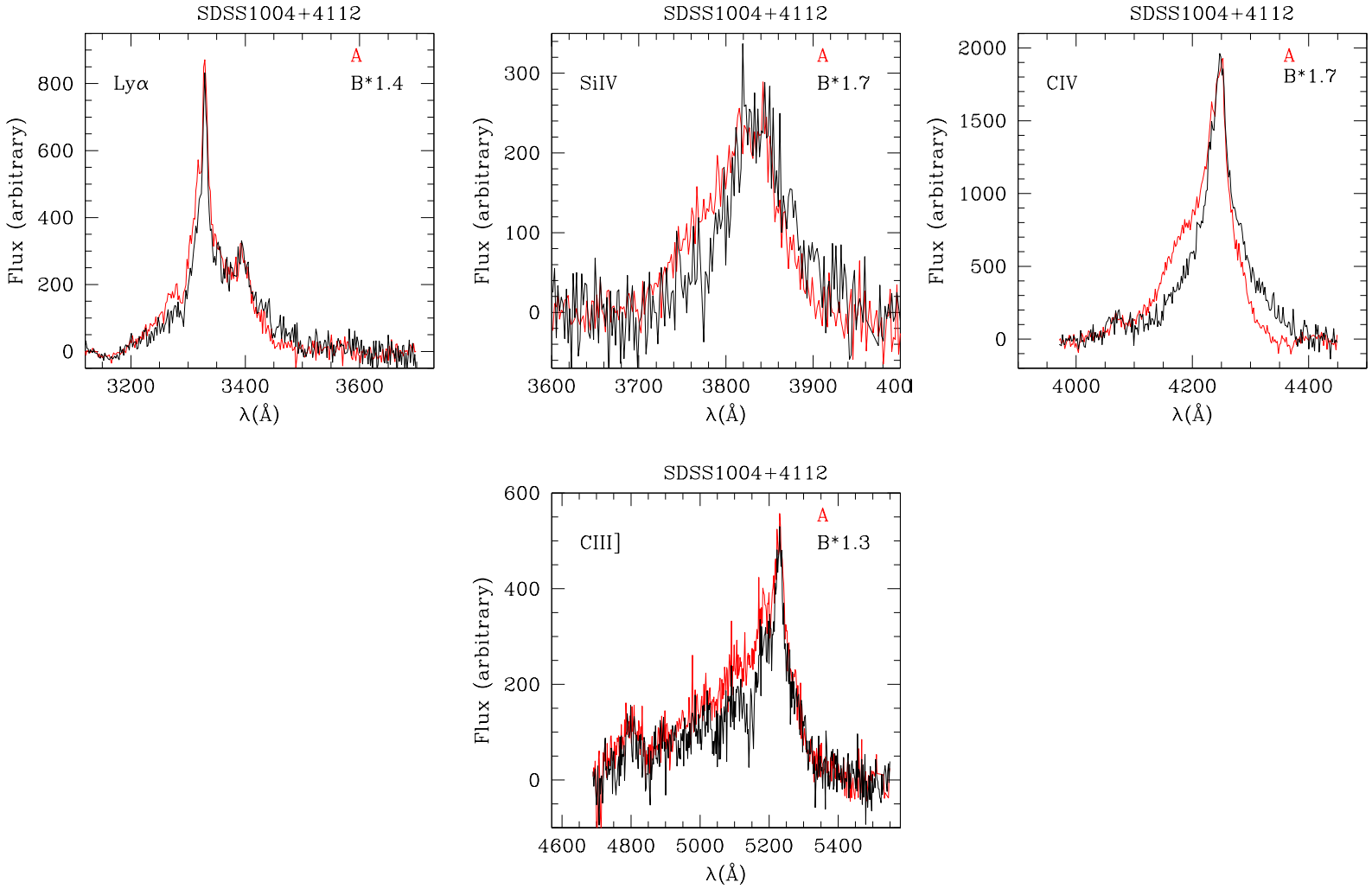

Fig. 4.— Lyα, SiIV, CIV, CIII] emission line profiles for SDSS1004+4112 vs. observed λ. The *red line* (*black line*) is the continuum-subtracted emission line for A (B multiplied by a factor to match the peak of A).

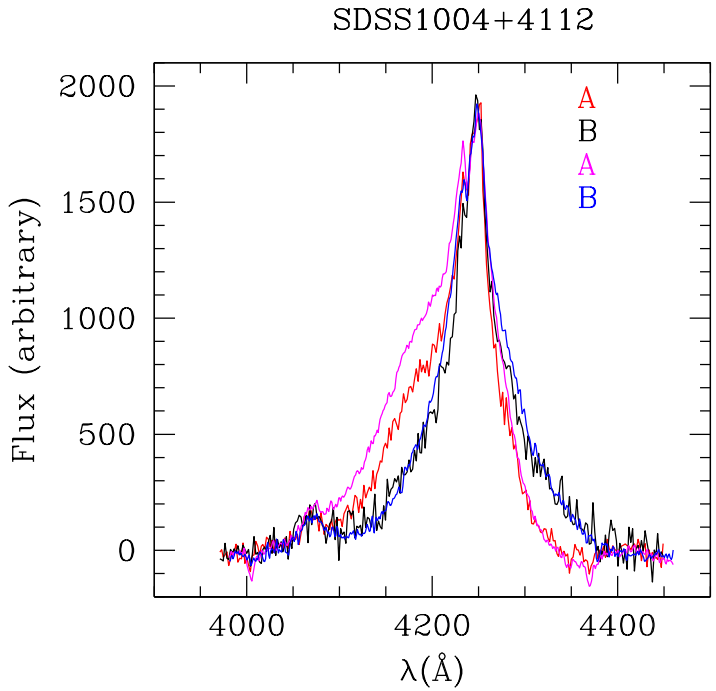

Fig. 5.— CIV emission line profile comparison for SDSS1004+4112. *Red* and *black* lines are A and B MMT spectra respectively, *magenta* and *blue* are A and B Keck spectra from Richards et al. (2004) respectively.

$A - B$ magnitude differences in the continuum and emission lines from VM12 or the literature are in Figure 6 (Table 1). The $A - B$ magnitude differences for the emission lines show no trend with wavelength (within uncertainties) and are distributed around $< A - B >= -0.52 \pm 0.07$ mag supporting the absence of dust extinction and defining the baseline for no microlensing magnification.

In 2004 the continuum difference curve from the spectra matched the no-microlensing baseline defined from the low ionization emission lines. With small offsets the broad-band based continuum data from Oguri et al. (2004) and Inada et al. (2003, 2005) also match the baseline for no microlensing. This lack of microlensing evidence in the continuum in 2004 (as the counterpart of the blue wing enhancements) seemed a serious setback to the microlensing hypothesis (Gómez-Álvarez et al. 2006).

The VM12 $A - B$ continuum difference measurements (Figure 6) from 2008 spectra strongly depart from the zero microlensing baseline with an increasing trend towards the blue that would include the X-ray measurements of Ota et al. (2006). The magnitude difference in the continuum is consistent with CASTLES broad-band data.

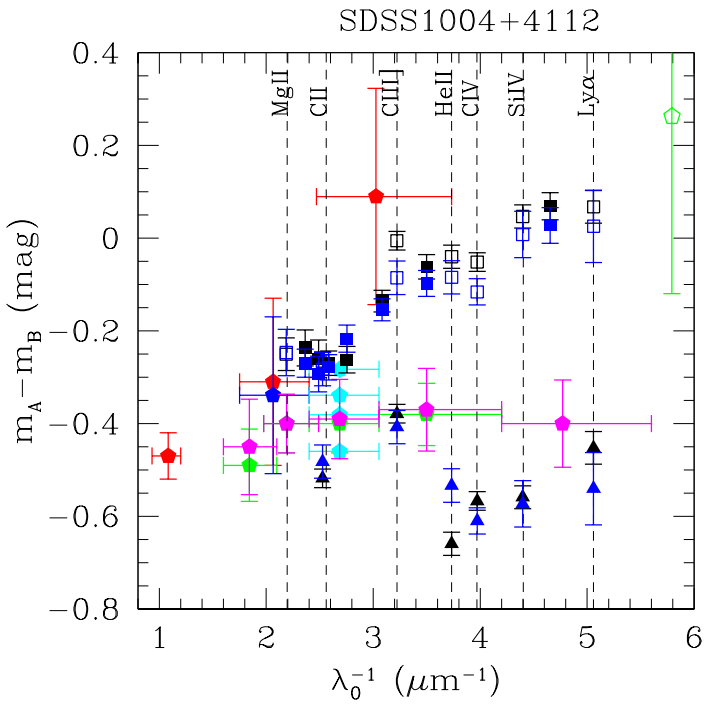

Fig. 6.— Magnitude differences $m_A - m_B$ vs λ_0^{-1} (λ in the lens galaxy restframe) for SDSS1004+4112. *Solid pentagons* are the integrated continuum obtained from (broad-band) CASTLES (*red*), Inada et al. (2003) (*green*), Inada et al. (2005) (*blue*), Oguri et al. (2004) (*magenta*), and Fohlmeister et al. (2008) (*cyan*). *Green open pentagons* are the X-ray data of Ota et al. (2006) (for display convenience, shifted in wavelength from 60 to 290 μm; i.e. from 28 to 5.8 μm^{-1} in the rest frame). *Black* and *blue squares* are the magnitude differences from the integrated continuum of the spectra (*solid*) and from the integrated fitted continuum under the emission lines (*open*) for two different exposures. *Black* and *blue triangles* are magnitude difference in the emission line cores.

The A-B continuum differences corrected for the time delay measured by Fohlmeister et al. (2008) change in the sequence: -0.460 ± 0.005 mag (2003-04), -0.283 ± 0.007 mag (2004-05), -0.339 ± 0.005 mag (2005-06), and -0.381 ± 0.007 mag (2006-07). The lowest value, -0.46 ± 0.005 mag, is close to the mean magnitude difference in the emission lines, -0.52 ± 0.07 mag, indicating that at this epoch (2003-04) the system underwent little microlensing.

Figure 7 shows a linear fit to the continuum data and the average of the emission line data. The magnitude difference variation in the continuum data (with a slope of $0.13 \pm 0.04\,\mathrm{mag}\,\mu\mathrm{m}^{-1}$) implies differences with respect to the emission lines of ~ 0.2 and ~ 0.5 mag at 7680 and 3320 Å respectively. The results are consistent with the trend indicated by the X-ray continuum data (Ota et al. 2006). Thus, the VM12 data indicate negligible dust extinction and evidence of chromatic microlensing. Conclusion: the hypothesis of microlensing to account for the enhancement in the blue wings is supported.

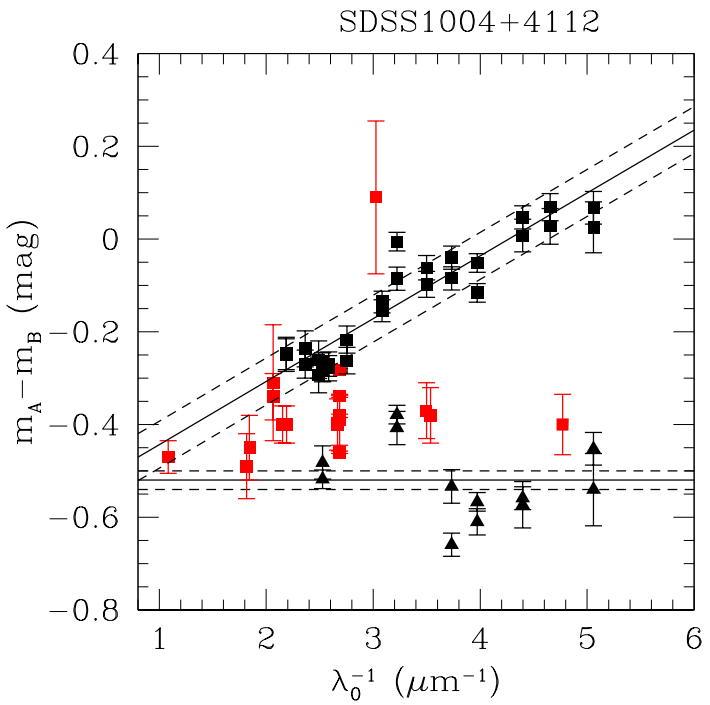

Fig. 7.— Model fitted to the data of Figure 6. *Squares* and *triangles* are continuum and NEL data, respectively. *Black lines* are the function fitted to the continua and the average of the emission line cores. *Dashed lines* are the standard deviations for the continuum fits and the standard error of the mean for the emission line cores.

Given the chromaticity, VM12 studied the structure of the accretion disk. They used ($\kappa_A = 0.48$, $\gamma_A = 0.59$) and ($\kappa_B = 0.48$, $\gamma_B = 0.48$) from Mediavilla et al. (2009) to obtain magnification maps for the A and B images. Applying this procedure to microlensing measurements at 3 different wavelengths from the MMT data (see Table 3), they obtained the 2D probability density functions (pdfs) in Figure 8 for both linear and logarithmic grids in r_s. From these distributions they obtained $r_s = 7 \pm 3$ lightdays ($18.1 \pm 7.8 \times 10^{15}$ cm) and $p = 1.1 \pm 0.4$ for the linear prior and $r_s = 6^{+4}_{-3}$ lightdays ($15.5^{+10.4}_{-7.8} \times 10^{15}$ cm) and $p = 1.0 \pm 0.4$ for the logarithmic prior. Although the value of p is consistent with the thin-disk theory, it agrees with the trend to have $p < 4/3$ (see Mediavilla et al. 2011; Blackburne et al. 2011). The microlensing estimate for the size also exceeds substantially the estimate obtained from thin-disk theory ($r_s \sim 0.3$ lightdays $= 0.78 \times 10^{15}$ cm, Mosquera & Kochanek 2011).

To study the impact of intrinsic variability on their results, VM12 compared the A-B difference they measured using the emission lines or the continuum at 12500Å (see Table 3), where microlensing and dust extinction should be insignificant. They found a difference between both measurements (a conservative upper bound to continuum variability) of 0.08 mag, implying an insignificant impact on estimates of r_s and p.

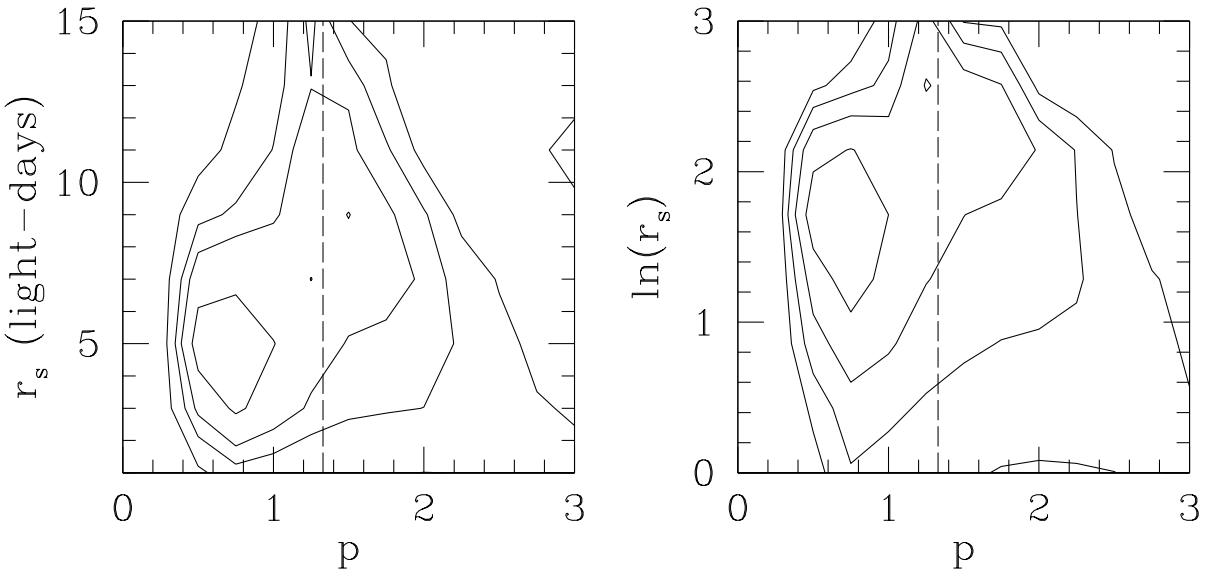

Fig. 8.— Two-dimensional pdfs from the measured chromatic microlensing for SDSS1004+4112 (Table 3) for both linear (*left*) and logarithmic (*right*) grids in r_s. Contours at 0.5σ, 1σ, 1.5σ, and 2σ respectively. From the pdfs,$r_s = 7 \pm 3\,\mathrm{light-days}(18.1 \pm 7.8 \times 10^{15}\mathrm{cm})$ and $p = 1.1 \pm 0.4$ for the linear prior and $r_s = 6^{+4}_{-3}\,\mathrm{light-days}(15.5^{+10.4}_{-7.8} \times 10^{15}\mathrm{cm})$ and $p = 1.0 \pm 0.4$ for the logarithmic prior. The *dashed line* is the value predicted by the thin-disk model ($p = 4/3$)

Table 3. SDSS1004+4112 chromatic microlensing

λ_c (Å)	$\Delta m_C - \Delta m_L$ [a] (mag)
3700	0.60 ± 0.02
6338	0.40 ± 0.02
12500	0.08 ± 0.04

[a] $(m_B - m_A)_C - (m_B - m_A)_L$

5. SDSS1029+2623

Inada et al. (2006) discovered the strong lens SDSS1029+2623. It contains two images A, B separated by $22\farcs5$ (the largest so far) at $z_s = 2.197$. Recently, Oguri et al. (2008) found a third image C $1\farcs8$ from B and several complex absorption systems in the emission lines. The lens is a cluster of galaxies at $z_L \sim 0.55$. (Fohlmeister et al. 2012) estimated a time delay for A and B of $\Delta t_{AB} = (744 \pm 10)$ days.

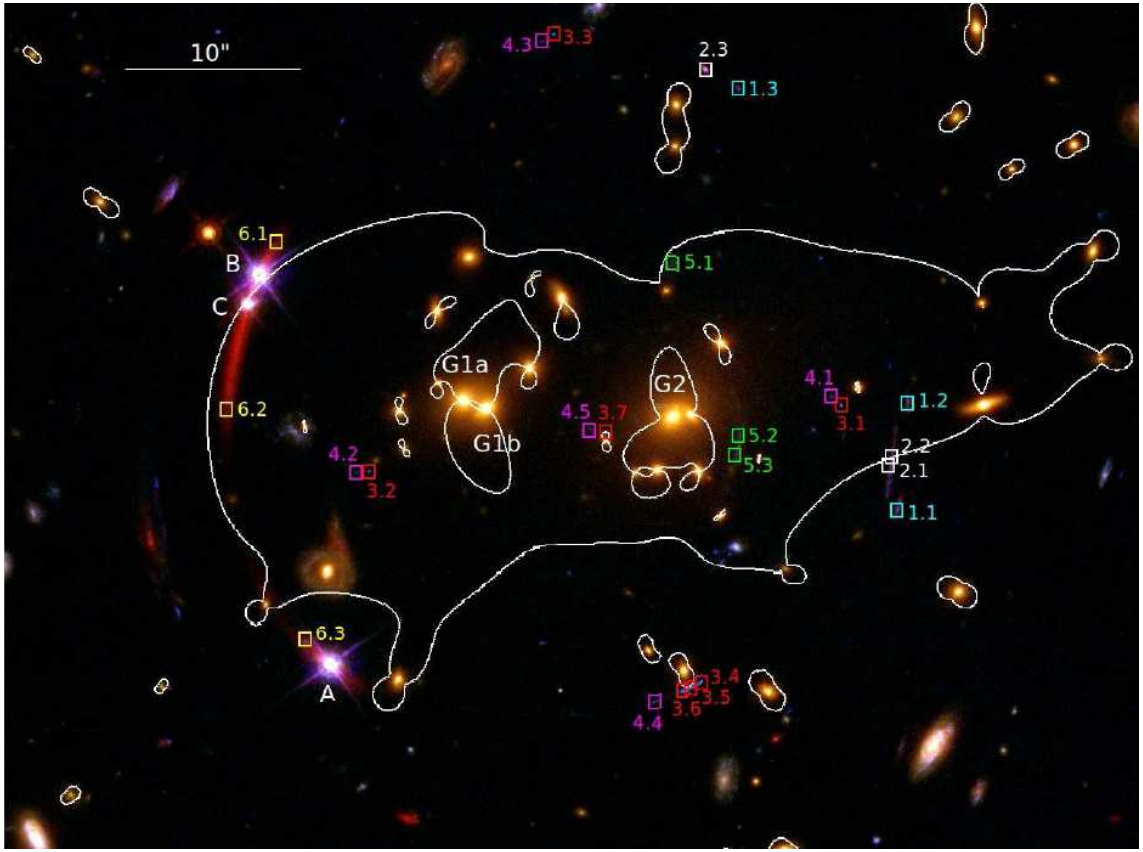

Fig. 9.— Color image with HST ACS/F475W, ACS/F814W, and WFC3/F160W data. North (East) is up (left). The quasar images are labeled A, B, and C. Squares with ID numbers are at the locations of identified multiple images. Galaxies G1a, G1b, G2 are the central galaxies of the lens cluster. Solid lines are the lensing critical curves for the Oguri et al. (2012) best-fit mass model.

The emission line profiles for A and B are similar for A and B (Figure 10), there are several groups of absorption line systems affecting Lyα and CIV that are associated with MgI/MgII/FeII absorption systems, as found by Oguri et al. (2008). There are also self-absorption systems associated with Lyα, SiIV, and CIV lines that are present in both components but with significant differences. In spite of this VM12 attempted to determine flux ratios by defining suitable integration windows to avoid the absorptions. In the case of CIII], the emission line profiles are almost identical in both components and show no absorption lines. The results derived from this line are most reliable.

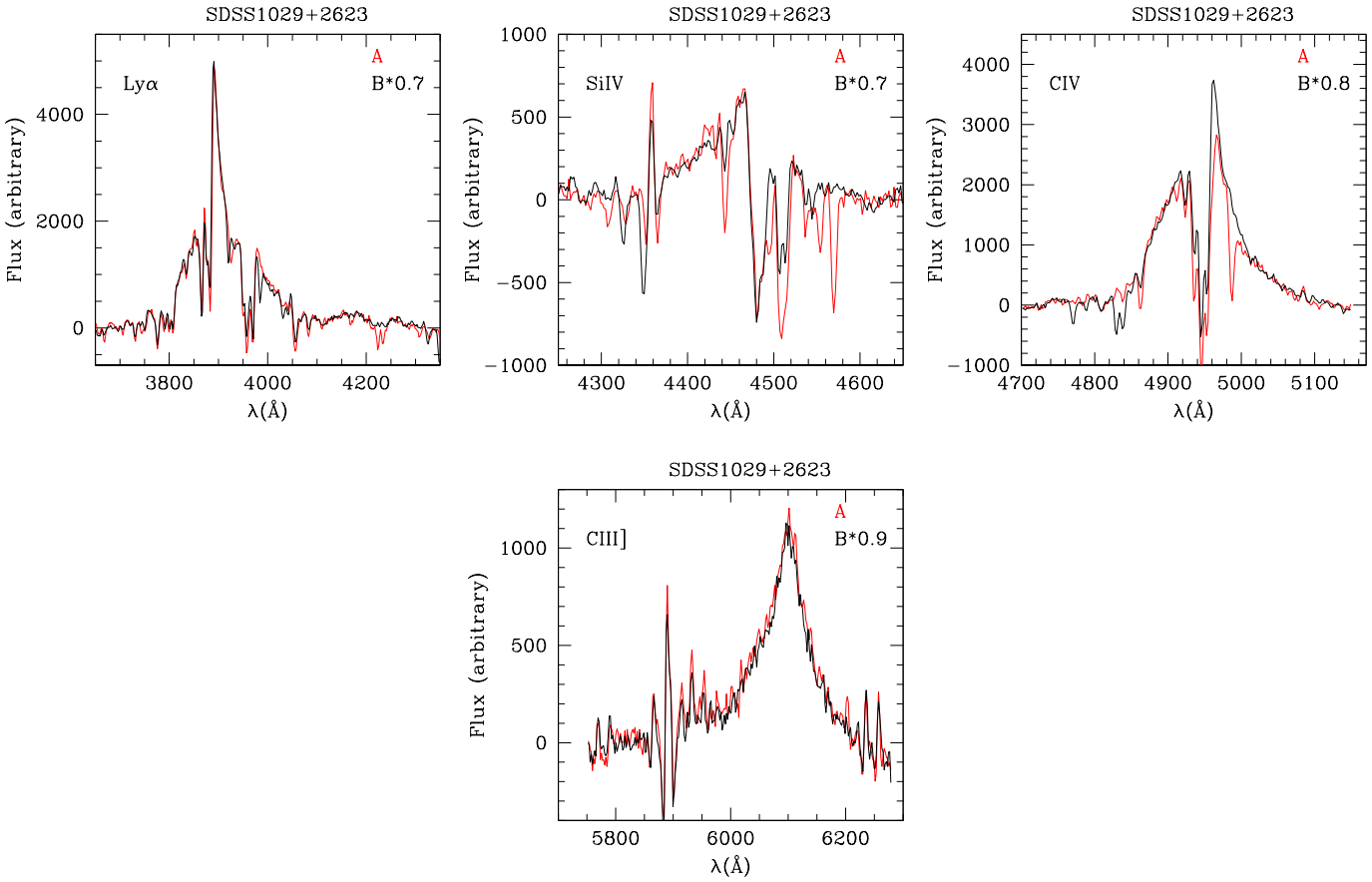

Fig. 10.— Lyα, SiIV, CIV, CIII emission line profiles for SDSS1029+2623 vs. observer λ. The *red lines black lines*) are continuum-subtracted emission lines for A (B). B was multiplied by a factor to match the peak of A. Each factor is shown in each panel. Sky lines are seen on both sides of CIII].

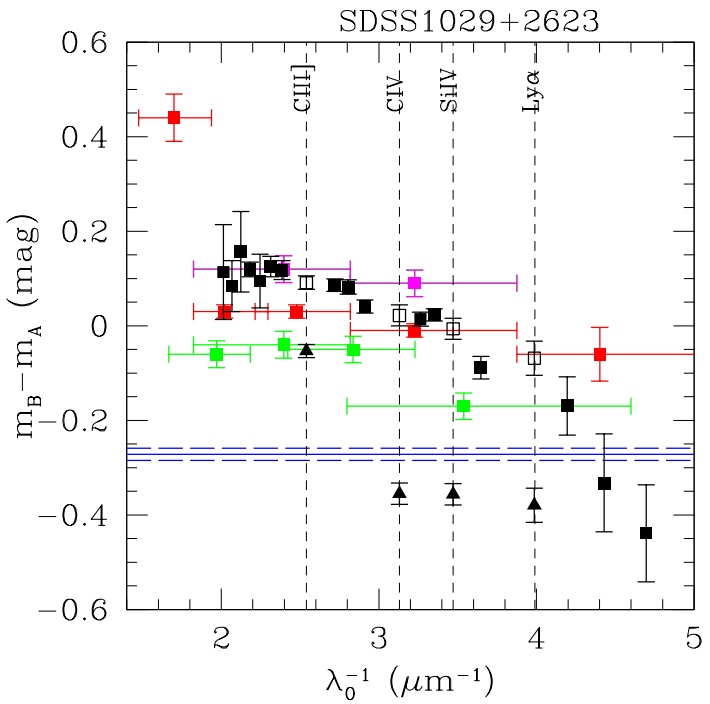

Fig. 11.— Magnitude differences $m_B - m_A$ vs λ_0^{-1} (λ in the lens galaxy restframe) for SDSS1029+2623. *Solid squares* are integrated continua, in color data from Inada et al. (2006) (*red*) and Oguri et al. (2008) (*green* and *magenta* are 2007 and 2008 data, respectively), and in *black* VM12 spectra. *Open black squares* are differences in the integrated fitted continua under the emission lines. *Black triangles* are magnitude differences in the emission line cores. The *blue line* is the magnitude difference and its error (*blue dashed lines*) at radio wavelengths (Kratzer et al. 2011).

The $B-A$ magnitude differences from the VM12 data (continuum and emission lines) compared to those obtained by Inada et al. (2006) and Oguri et al. (2008) are in Fig. 11.

Their continuum flux ratio agrees with the data for the Keck g and K broadband filters from Oguri et al. (2008), taken at the same epoch. However, there is a difference of ~ 0.1 mag with data at other epochs. Thus, there was variability in the continuum between 2007 and 2008 (another peculiar feature is that the measurement in the z band (Inada et al. 2006) is ~ 0.3 mag above all the other broad-band measurements).

The strong chromaticity of the continuum flux ratio (about 0.4 mag) that exceeds the ~ 0.1 mag global offset between continuum flux ratios at different epochs excludes intrinsic continuum variability. Dust extinction also cannot explain the chromaticity as the flux ratio from radio data agrees with the flux ratio of the bluest continuum, contrary to expectations for extinction. Thus, microlensing is the more likely explanation and is supported by the agreement of the flux ratios inferred from CIV, SiIV, and Lyα with the radio flux ratio.

However, the flux ratio inferred from the other emission line, CIII] which presents the smoothest line profile, shows a large offset with respect to the baseline defined by the radio data that disagrees with the microlensing hypothesis. Assuming chromatic microlensing the same steps as for SDSS1004+4112 would be available to estimate the size and temperature profile of the QSO source in SDSS1029+2623. However, lens modeling in this system is not yet sufficiently refined for this purpose Oguri et al. (2012).

6. HE1104-1805

Wisotzki et al. (1993) discovered the double HE1104-1805. The lens galaxy was detected by Courbin et al. (1998) at $z_l = 0.729$. Image A is $1\farcs1$ from the main lens galaxy. Variability in the continuum was detected in spectra by Wisotzki et al. (1995) (optical), Courbin et al. (1998) (near infrared), and Chartas et al. (2009) (X-ray). Poindexter et al. (2007) monitored the system between 2003 and 2006, concluding that the magnitude difference in the optical bands has changed from -1.7, when the lens was discovered, to -1.2 in their optical data (2006). Their estimated time delay is $152.2^{+2.8}_{-3.0}$ (1 σ) days.

The emission line profiles of both images are very similar, although some slight differences appear in the broad components of CIV and SiIV (Figures 12 and 13). Lyα is only seen in the VM12 MMT spectra. The profile of the MgII emission line was asymmetric both in A and B. CIII] showed strong absorption lines in both the BEL and NEL. In their higher-SNR VLT data it was clear that A shows several absorption lines, none of them present in the B spectrum. The profiles of CIV and SiIV emission lines show a slight enhancement in the red wing of A compared to those of B both in MMT and VLT data. Such wing enhancements that are visible only in high ionization lines might be evidence of microlensing.

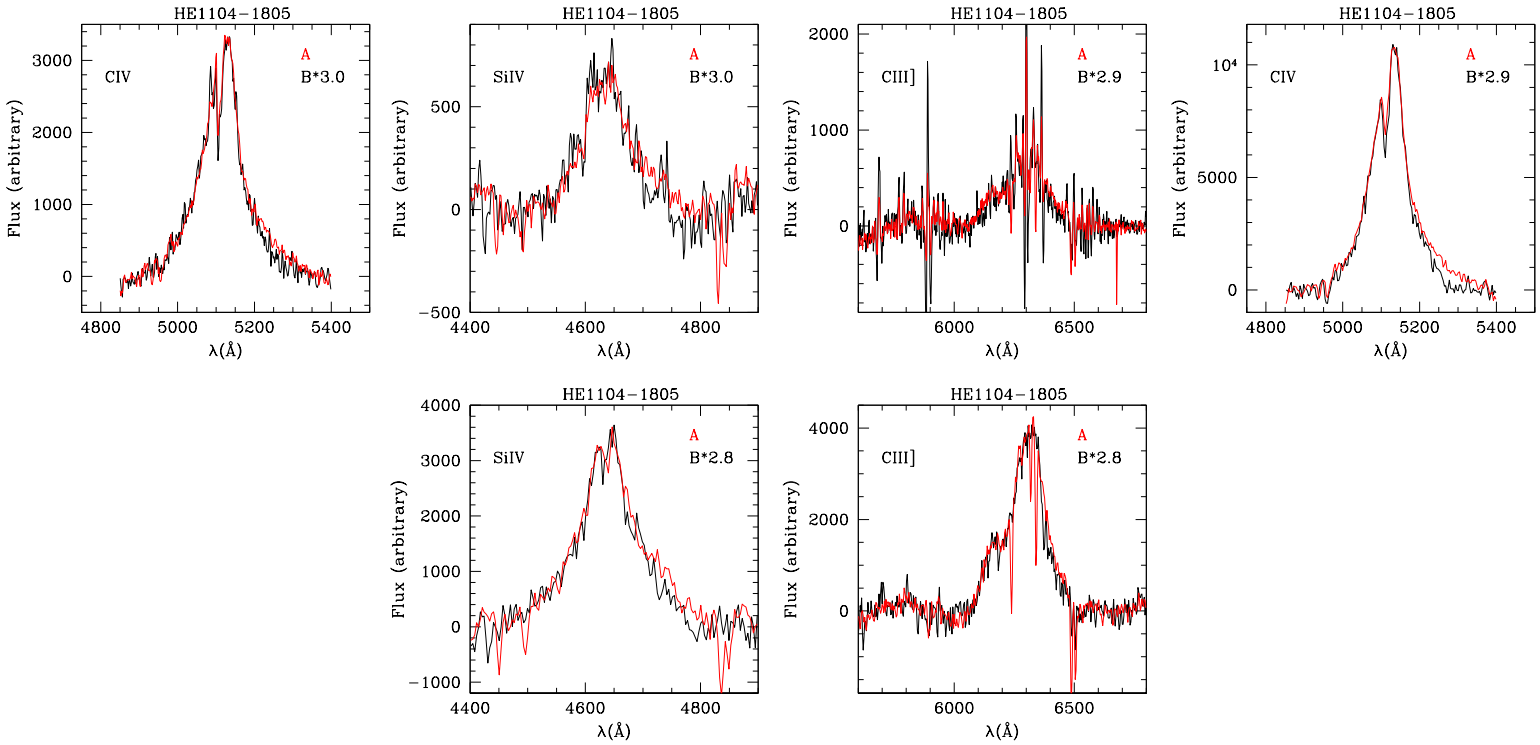

Fig. 12.— CIV, SiIV, CIII] emission line profiles for HE1104-1805 vs. observed λ. *First 3 panels* are MMT spectra. The *red line* represents the continuum-subtracted emission lines for A. The *black line* represents the continuum subtracted emission line for B multiplied by a factor to match the peak of A. The factors are shown in each panel. *Last 3 panels* similar to first panels but for VLT spectra.

Figure 14 shows the magnitude differences in the continuum and in the emission lines, including data from the literature (Table 1). The mean B-A magnitude difference ($< B - A >= -1.13 \pm 0.02$ mag) corresponding to the emission lines from the MMT and VLT spectra is consistent with the values derived by Wisotzki et al. (1995) (~ -1.14 mag) and Courbin et al. (2000) (-1.16 ± 0.04 mag). These values are also in agreement with the value estimated from IR data -1.13 ± 0.03 mag (Poindexter et al. 2007). Conclusion: the cores of the emission lines are not microlensed, and little extinction is present.

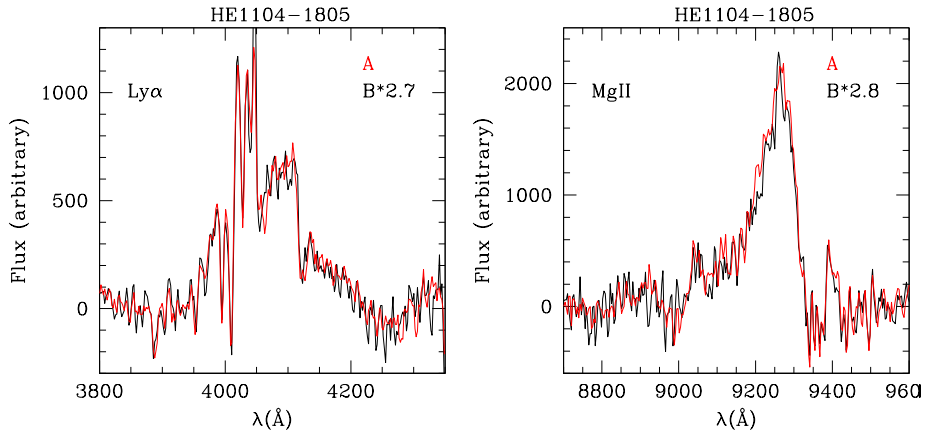

Fig. 13.— Lyα, MgII emission line profiles for HE1104-1805 vs. observed λ. The *red line* (*Black line*) represents continuum subtracted emission lines for A (B). B was multiplied by 2.7 to match the peak of A (*red line*).

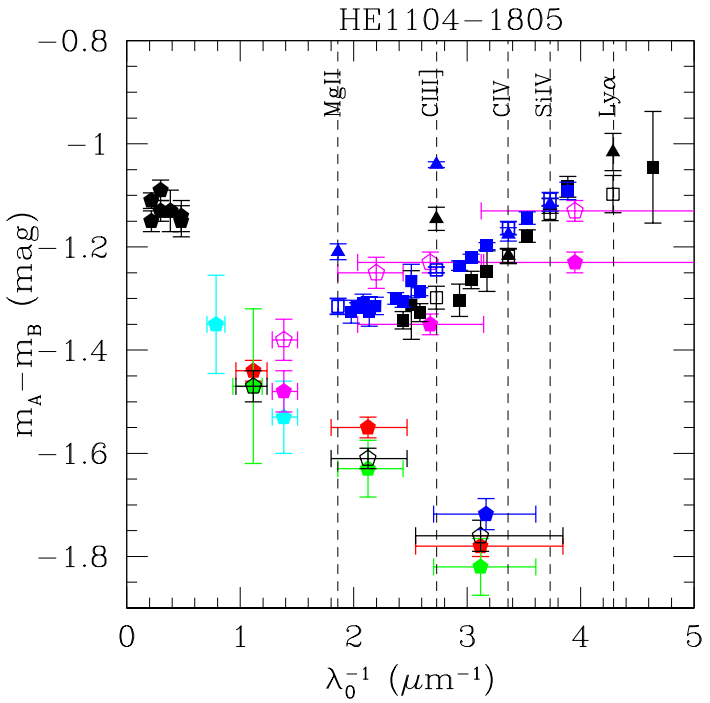

Fig. 14.— Magnitude differences $m_A - m_B$ vs λ_0^{-1} (λ in the lens galaxy restframe) for HE1104-1805. *Black and blue* are magnitude differences from MMT and VLT spectra respectively. *Solid squares* are magnitude differences in the continuum, *open squares* in the integrated continuum under the emission line, and *solid triangles* in the emission line core. The broadband data from other authors are plotted as *pentagons* in different colors representing: CASTLES (*red*), Lehár et al. (2000) (*green*), Courbin et al. (1998) (*cyan*), Schechter et al. (2003) (*blue*), Falco et al. (1999) (*open black*), Poindexter et al. (2007) Spitzer IRAC (*solid black*). *Magenta pentagons* represent the optical broadband data obtained by Poindexter et al. (2007) with (*solid*) and without (*open*) time-delay correction.

The $B - A$ magnitude differences in the continuum from the MMT and VLT spectra show a slope that agrees with optical broad-band data of 2006 (Poindexter et al. 2007)[1]. Broad-band data obtained several years earlier (Falco et al. 1999; Lehár et al. 2000; Courbin et al. 2000; Schechter et al. 2003) are consistent (slope $-0.16 \pm 0.03\,\mathrm{mag}\,\mu\mathrm{m}^{-1}$) but are very different from the VM12 and Poindexter et al. (2007) data.

Linear fits to the magnitude differences of continua are in Figure 15. The slope for the magnitude differences in the emission lines and the IR data was $0.00 \pm 0.06\,\mathrm{mag}\,\mu\mathrm{m}^{-1}$, consistent with no extinction and in agreement with results from near-IR spectra of Courbin et al. (2000) ($\Delta E < 0.01$) and in Falco et al. (1999) ($\Delta E = 0.07 \pm 0.1$) from broadband photometry. The continuum data from the literature are fitted in two subsets: 1992-1994 data with a slope of $-0.16 \pm 0.03\,\mathrm{mag}\,\mu\mathrm{m}^{-1}$ and more recent data from Poindexter et al. (2007) with a slope of $0.08 \pm 0.06\,\mathrm{mag}\,\mu\mathrm{m}^{-1}$. The slope of the linear fit to the VM12 2008 continuum data (MMT+VLT), $0.12 \pm 0.02\,\mathrm{mag}\,\mu\mathrm{m}^{-1}$, agrees with 0.08 ± 0.06 for the 2006 data of Poindexter et al. (2007), but is very different from 1992-1994 (broadband data) $-0.16 \pm 0.03\,\mathrm{mag}\,\mu\mathrm{m}^{-1}$. Thus, microlensing in HE1104-1805 induced a large change in continuum slope. To explain the slope of the continuum for the 2006-2008 period, VM12 combined chromatic microlensing in both A and B. For instance, they consider the combination of two events of magnification in both A and B with a progressive increase in the strength of the B event from 1994 to 2008.

[1] As VM12 could not correct their data for a time delay, they considered both the time-delay corrected and uncorrected optical data obtained by Poindexter et al. (2007). The lens galaxy continuum is very faint, so it cannot contaminate their spectra.

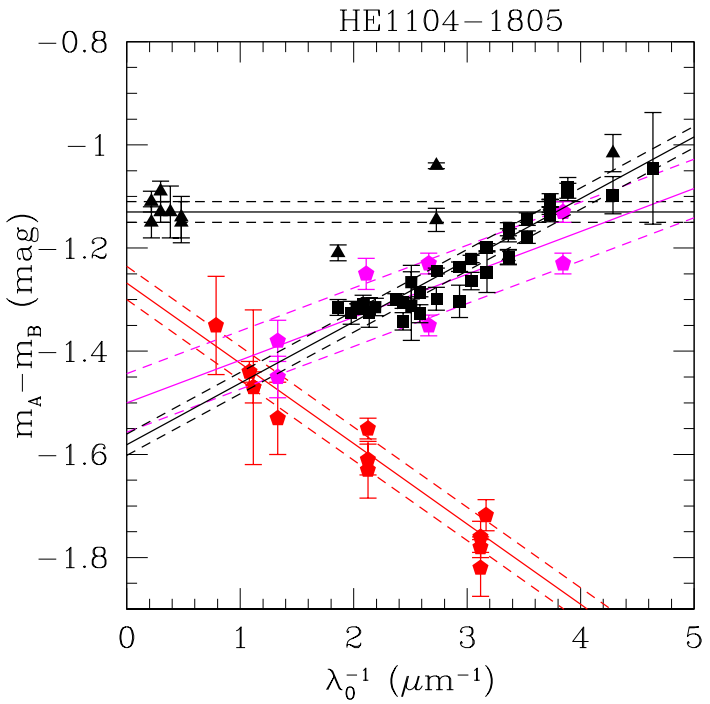

Fig. 15.— Model fitted to the data shown in Figure 14. *Black lines* are the fitted function to the continua (*squares*) for MMT and VLT data and the average of the emission line cores (*triangles*) respectively. The *red line* is the function fitted to the broadband data in the literature (CASTLES; Lehár et al. 2000; Courbin et al. 1998; Falco et al. 1999; Schechter et al. 2003) at the same epoch. The *magenta line* is the function fitted to the broadband data of Poindexter et al. (2007) with and without time-delay correction. The IR data of Poindexter et al. (2007) are the *black triangles*. *Dashed lines* are standard deviations for each fit (continua and broadband data) and the error of the mean for the emission line cores.

VM12 used the detected microlensing chromaticity to study the structure of the accretion disk in HE1104-1805. They used 3 sets of data: the VM12 VLT continuum data, the Poindexter et al. (2007) data corrected for time delay and the average of the data from Courbin et al. (1998), Falco et al. (1999), Lehár et al. (2000), and Schechter et al. (2003) that consistently follow a common trend with wavelength. Table 4 shows the microlensing measurements for each dataset. To compute the microlensing maps VM12 used projected densities and shears for each lens image of ($\kappa_A = 0.64$, $\gamma_A = 0.52$) and ($\kappa_B = 0.33$, $\gamma_B = 0.21$) as in Mediavilla et al. (2009).

The resulting pdfs are in Fig. 16, and the expected values and uncertainties in Table 5.

Table 4. HE1104-1805 chromatic microlensing

λ_c (Å)	$\Delta m_C - \Delta m_L$[a] (mag)
4380	-0.09 ± 0.02
6470	-0.21 ± 0.02
12500	-0.34 ± 0.04
5550	0.65 ± 0.03
8140	0.46 ± 0.03
15500	0.32 ± 0.03
3700	-0.15 ± 0.02
6338	0.16 ± 0.02
12500	0.31 ± 0.02

Table 5. HE1104-1805 accretion disk parameters (1σ error)

Data	Linear		Logarithmic	
	p	$r_s \times 10^{15}$ (cm)	p	$r_s \times 10^{15}$ (cm)
VM12	1.7 ± 0.8	28.5 ± 10.4	1.7 ± 0.8	23.3 ± 5.2
Average Lit.	1.1 ± 0.7	23.3 ± 10.4	0.9 ± 0.2	10.4 ± 5.2
Poindexter et al. (2007)	0.8 ± 0.3	23.3 ± 7.8	1.1 ± 0.6	18.1 ± 5.2
Intersection	0.6 ± 0.1	15.5 ± 5.2	0.7 ± 0.1	15.5 ± 2.6

The pdfs corresponding to the MMT/VLT (Fig.16a) and to the Poindexter et al. (2008) data (Fig.16c) are not as concentrated near the maximum of the pdf as in the case of the broad-band data (Fig 16b). These pdfs may present a secondary maximum (perhaps due to the complexity of the microlensing phenomenon corresponding to this epoch) and, individually considered, are not very conclusive. However, the product pdf strongly increases the concentration of the probability near the maximum and the significance of the estimates: $r_s = 6 \pm 2$ lightdays $(15.5 \pm 5.2 \times 10^{15}\,\mathrm{cm})$, $p = 0.7 \pm 0.1$ for the linear prior and $r_s = 6^{+2}_{-1}$ lightdays $(15.5^{+5.2}_{-2.6} \times 10^{15}\,\mathrm{cm})$, $p = 0.7 \pm 0.1$ for the logarithmic prior. The VM12 r_s estimates correspond to one half-light radius at the central wavelength of B, $R_{1/2}(\lambda 4311) = 8 \pm 2$ lightdays $(76 \pm 19 \times 10^{17}\,\mathrm{cm})$. This value is in good agreement with the results in Muñoz et al. (2011) based on HST data and with those in Poindexter et al. (2008) based on photometric monitoring.

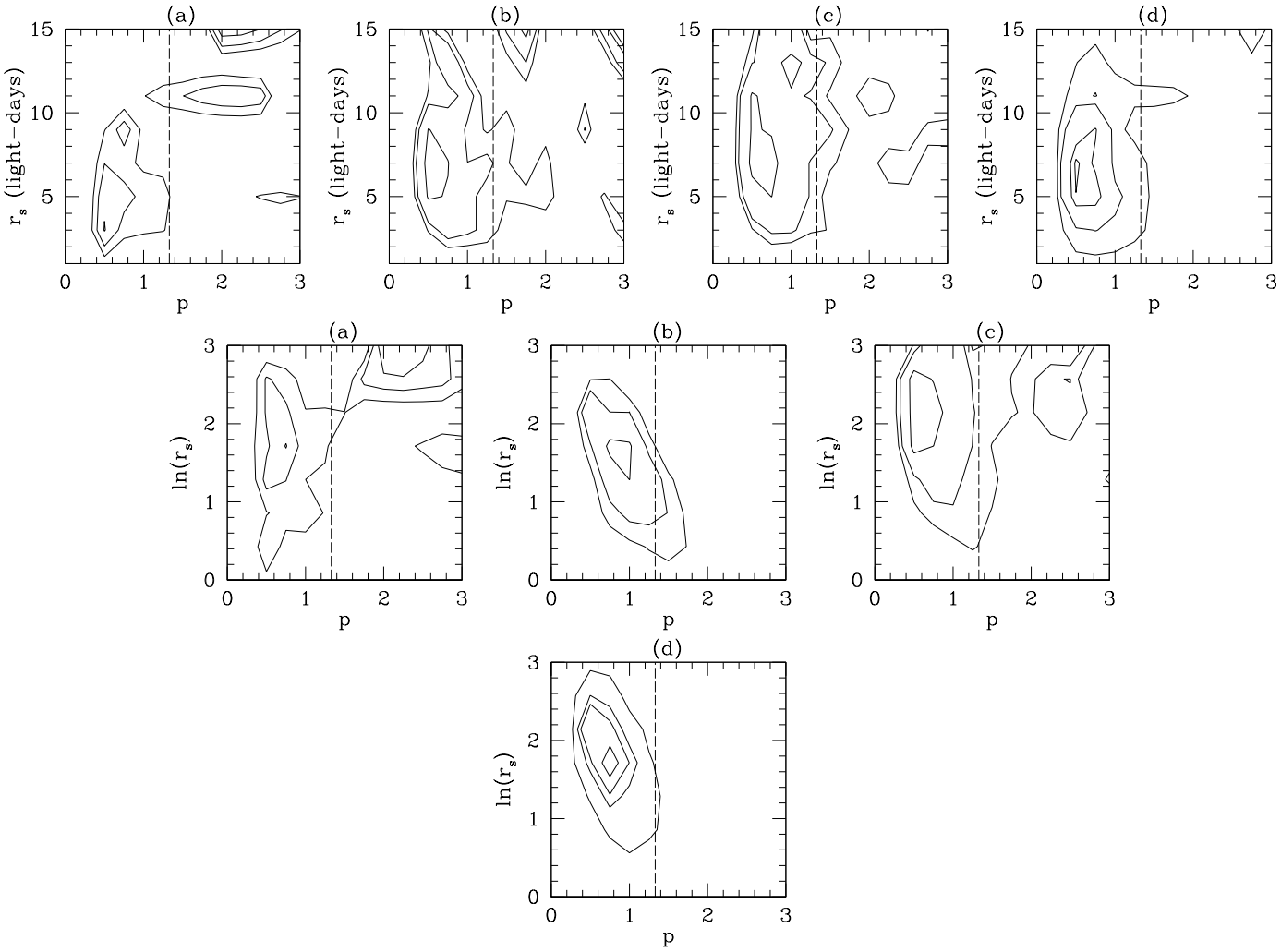

Fig. 16.— Two-dimensional pdfs for the measured chromatic microlensing of HE1104-1805 (Table 4) for both linear (*top*) and logarithmic (*bottom*) grids in r_s. Contours are 0.5σ, 1σ, and 1.5σ confidence levels respectively. From *left* to *right* pdfs for: MMT/VLT data (a), average of broadband data previous to 2003 (b), Poindexter et al. (2007) data corrected by time delay (c), and the intersection of the 3 previous maps (d).

7. CONCLUSIONS

- The method of VM12 allows a separation of microlensing from dust extinction without a model for the lens system. VM12 demonstrated the method for the most complicated cases: doubly-imaged QSOs.

- VM12 tested the hypothesis that the cores of emission lines do not vary with time by comparing their magnitude differences in the emission lines with the literature, obtained at different epochs, including values corrected for measured time-delays. They conclude that they are nearly constant in time. Thus, except in cases where extinction is significant, the magnitude differences in the emission line cores are reliable estimators of the intrinsic magnitude differences unaffected by microlensing.

- VM12 estimated the impact of time delays in their microlensing measurements. In the worst case scenario (SDSS1004+4142 and SDSS1029+2623) a time delay can introduce variabilities $\lesssim 0.2$ mag and chromaticities $\lesssim 0.1$ mag. Their measurements for those objects were at least twice these estimated values.

- Differences in the wings of the CIV and SiIV broad emission line profiles are found in A and B images of SDSS1004+4112, as detected previously by Richards et al. (2004), but the enhancement in the blue wing is smaller than observed in 2004. In HE1104-1805 they detected a slight enhancement in the red wings of CIV and SiIV in image A with respect to image B.

- The average microlensing magnification free from extinction was obtained as the difference in magnitudes between the emission lines and the continuum. The latter was obtained directly from the spectra with no contamination by the lens galaxy. Significant chromatic microlensing was detected in SDSS1004+4112, SDSS1029+2623, and HE1104-1805.

REFERENCES

Abajas, C., Mediavilla, E., Muñoz, J.A., Popović, L.Ć., Oscoz, A. 2002, ApJ, 576, 640

Abajas, C., Mediavilla, E., Muñoz, J.A., Gómez-Álvarez, P., Gil-Merino, R. 2007, ApJ, 658, 748

Agol, E., Jones, B, Blaes, O. 2000, ApJ, 545, 657

Bernstein, G., Fischer, P., Tyson, J.A., Rhee, G. 1997, ApJ, 483, L79

Blackburne, J.A., Pooley, D., Rappaport, S. and Schechter, P.L. 2011, ApJ, 729, 34

Bradac, M., Schneider, P., Steinmetz, M., Lombardi, M., King, L.J., Porcas, R. 2002, A&A, 388, 373

Cardelli, J. A. and Clayton, G. C. and Mathis, J. S. 1989, ApJ, 345, 245

Chartas, G., Agol, E., Eracleous, M., Garmire, G., Bautz, M.W., Morgan, N. D. 2002, ApJ, 568, 509

Chartas, G., Eracleous, M., Agol, E., Gallagher, S. C. 2004, ApJ, 606, 78

Chartas, G., Kochanek, C. S., Dai, X., Poindexter, S., and Garmire, G. 2009, ApJ, 693, 174

Chiba, M. 2002, ApJ, 565, 17

Colley, W.N., Schild, R.E., Abajas, C., Alcalde, D., Aslan, Z., Barrena, R., Dudinov, V., Khamitov, I., Kjernsmo, K., Lee, H.J., Lee, J., Lee, M.G., Licandro, J., Maoz, D., Mediavilla, E., Motta, V., Muñoz, J., Oscoz, A., Serra-Ricart, M., Sinelnikov, I., Stabell, R., Teuber, J., Zheleznyak, A. 2002, ApJ, 565, 105

Courbin, F., Lidman, C., Magain, P. 1998, A&A, 330, 57

Courbin, F., Lidman, C., Meylan, G., Kneib, J.-P., Magain, P. 2000, A&A, 360, 853

Conner, Samuel R.; Lehar, Joseph; Burke, Bernard F. 1992, ApJ, 387, L61

Dalal, N., Kochanek, C.S. 2002, ApJ, 572, 25

Dolan, J.F., Michalitsianos, A.G., Thompson, R. W.; Boyd, P. T.; Wolinski, K. G.; Bless, R. C.; Nelson, M. J.; Percival, J. W.; Taylor, M. J.; Elliot, J. L.; van Citters, G. W. 1995, ApJ, 442, 87

Elvis, M. 2000, ApJ, 545, 63

Falco, E.E., Impey, C.D., Kochanek, C.S., Lehár, J., McLeod, B.A., Rix, H.-W., Keeton, C.R., Muñoz, J.A., Peng, C.Y. 1999, ApJ, 523, 617

Filippenko, A.V. 1989, ApJ, 338, L49

Fitte, C., Adam, G. 1994, A&A, 282, 11

Floyd, D.J.E., Bate, N.F., Webster, R.L. 2009, MNRAS, 398, 233

Fohlmeister, J., Kochanek, C. S., Falco, E. E., Wambsganss, J., Oguri, M., Dai, X. 2012. A Two Year Time Delay for SDSS J1029+2623. ArXiv e-prints arXiv:1207.5776.

Fohlmeister, J., Kochanek, C.S., Falco, E.E., Morgan, C.W., Wambsganss, J. 2008, ApJ, 676, 761

Fohlmeister, J., Kochanek, C.S., Falco, E.E.,Wambsganss, J., Morgan, N., Morgan, C.W., Ofek, E.O., Maoz, D., Keeton, C.R., Barentine, J.C., Dalton, G., Dembicky, J., Ketzeback, W. McMillan, R., Peters, C.S. 2007, ApJ, 662, 62

Goicoechea, L. J., Gil-Merino, R., Ullan, A., Serra-Ricart, M., Muñoz, J. A., Mediavilla, E., Gonzalez-Cadelo, J., Oscoz, A., 2005, ApJ, 619, 19

Goicoechea, L. J.; Gil-Merino, R.; Ullan, A. 2005, MNRAS, 360, L60

Gómez-Álvarez, P., Mediavilla, E., Muñoz, J.A., Arribas, S., Sánchez, S.F., Oscoz, A., Prada, F., Serra-Ricart, M. 2006, ApJ, 645, L5

Gómez-Álvarez, P., Mediavilla, E., Sánchez, S.F., Arribas, S., Wisotzki, L., Wambsganss, J., Lewis, G., Muñoz, J.A. 2004, AN, 204, 132

Gorenstein, M. V., Cohen, N. L., Shapiro, I. I., Rogers, A. E. E., Bonometti, R. J., Falco, E. E., Bartel, N., and Marcaide, J. M. 1988, ApJ, 334, 42

Green, P.J. 2006, ApJ, 644, 733

Goicoechea, L. J., Shalyapin, V. N., Gil-Merino, R., and Ullán, A. 2008, A&A, 492, 411

Goicoechea, L. J. 2002, MNRAS, 334, 905

Hagen, H.-J., Reimers, D. 2000, A&A, 357, L29

Hamann, F., Barlow, T.A., Beaver, E.A., Burbidge, E.M., Cohen, R.D., Junkkarinen, V., Lyons, R. 1995, ApJ, 443, 606

Haschick, A.D., Moran, J.M., Reid, M.J., Davis, M., Lilley, A. E. 1981, ApJ, 243, L57

Howarth, I.D., Murray, J., Mills, D., Berry, D.S. 2004, Starlink User Note 50.24, Rutherford Appleton Laboratory.

Hutchings, J.B. 2003, AJ, 126, 24

Inada, N., Oguri, M., Pindor, B., Hennawi, J.F., Chiu, K., Zheng, W., Ichikawa, S.-I., Gregg, M.D., Becker, R.H.; Suto, Y., Strauss, M.A., Turner, E.L., Keeton, C.R., Annis, J., Castander, F.J., Eisenstein, D.J., Frieman, J.A., Fukugita, M., Gunn, J.E., Johnston, D.E., Kent, S.M., Nichol, R.C., Richards, G.T., Rix, H.-W., Sheldon, E.S., Bahcall, N.A., Brinkmann, J., Ivezić, Z., Lamb, D.Q., McKay, T.A., Schneider, D.P., York, D.G. 2003, Nature, 426, 810

Inada, N., Oguri, M., Morokuma, T., Doi, M., Yasuda, N., Becker, R.H., Richards, G.T., Kochanek, C.S., Kayo, I., Konishi, K., Utsunomiya, H., Shin, M.-S., Strauss, M.A., Sheldon, E.S., York, D.G.; Hennawi, J.F., Schneider, D.P., Dai, X., Fukugita, M. 2006, ApJ, 653, L97

Inada, N., Oguri, M., Keeton, C.R., Eisenstein, D.J., Castander, F.J., Chiu, K., Hall, P.B., Hennawi, J.F., Johnston, D.E., Pindor, B., Richards, G.T., Rix, H.-W., Schneider, D.P., Zheng, W. 2005, PASJ, 57, L7

Inada, N., Oguri, M., Falco, E.E., Broadhurst, T.J., Ofek, E.O., Kochanek, C.S., Sharon, K., Smith, G.P. 2008, PASJ, 60, L27

Ivezić, Z., Lupton, R.H., Schlegel, D., Boroski, B., Adelman-McCarthy, J., Yanny, B., Kent, S., Stoughton, C., Finkbeiner, D., Padmanabhan, N., Rockosi, C.M., Gunn, J.E., Knapp, G.R., Strauss, M.A., Richards, G.T., Eisenstein, D., Nicinski, T., Kleinman, S.J., Krzesinski, J., Newman, P.R., Snedden, S., Thakar, A.R., Szalay, A., Munn, J.A., Smith, J.A., Tucker, D., Lee, B.C. 2004, Astronomische Nachrichten, 325, 583

Jovanović, P., Zakharov, A. F., Popović, L. Ć.; Petrović, T. 2008, MNRAS, 386, 397

Kaspi, S., Smith, P.S., Maoz, D., Netzer, H., Jannuzi, B.T. 1996, ApJ, 471, L75

Kaspi, S., Brandt, W. N., Maoz, D., Netzer, H., Schneider, D.P., Shemmer, O. 2007, ApJ, 679, 997

Keeton, C.R. 2002, ApJ, 575, L1

Kochanek, C.S. (2004), ApJ, 605, 58

Kochanek, C.S., and Dalal, N. (2004), ApJ, 610, 69

Kochanek, C.S., Morgan, N.D., Falco, E.E., McLeod, B.A., Winn, J.N., Dembicky, J., Ketzeback, B. (2006), ApJ, 640, 47

Kratzer, R.M., Richards, G.T., Goldberg, D.M., Oguri, M., Kochanek, C.S., Hodge, J.A., Becker, R.H., and Inada, N. (2011), arXiv 1008.2315 Kochanek, C.S., and Dalal, N. (2004), ApJ, 610, 69

Lamer, G., Schwope, A., Wisotzki, L., Christensen, L. 2006, A&A, 454, 493

Lehár, J., Falco, E.E., Kochanek, C.S., McLeod, B.A., Muñoz, J.A., Impey, C.D., Rix, H.-W., Keeton, C.R., Peng, C.Y. 2000, ApJ, 536, 584

Lewis, G.F., Ibata, R.A. 1998, ApJ, 501, 478

Lewis, G.F., Ibata, R.A. 2004, MNRAS, 355, 106

Marziani, P., Sulentic, J.W., Negrete, C.A., Dultzin, D., Zamfir, S., Bachev, R., 2010, MNRAS, 409, 1033

Mathur, S., Elvis, M., Wilkes, B. 1999, ApJ, 519, 605

Mao, S., Schneider, P. 1998, MNRAS, 295, 587

Mediavilla, E., Muñoz, J.A., Kochanek, C.S., Falco, E.E., Arribas, S., Motta, V. 2005, ApJ, 619, 749

Mediavilla, E., Muñoz, J.A., Lopez, P., Mediavilla, T., Abajas, C., González-Morcillo, C., Gil-Merino, R. 2006, ApJ, 653, 942

Mediavilla, E., and Muñoz, J.A., Falco, E., Motta, V., Guerras, E., Canovas, H., Jean, C., Oscoz, A., Mosquera, A.M. 2009, ApJ, 706, 1451

Mediavilla, E., Muñoz, J.A., Kochanek, C.S., Guerras, E., Acosta-Pulido, J., Falco, E., Motta, V., Arribas, S., Manchado, A., Mosquera, A. 2011, ApJaccepted

Metcalf, R.B., Madau, P. 2001, ApJ, 563, 9

Metcalf, R.B., Zhao, H.S. 2002, ApJ, 567, L5

Morgan, C.W., Eyler, M.E., Kochanek, C.S., Morgan, N.D., Falco, E.E., Vuissoz, C., Courbin, F., Meylan, G. 2008, ApJ, 676, 80

Morgan, C.W., Kochanek, C.S., Morgan, N.D., Falco, E.E. 2010, ApJ, 712, 1129

Mosquera, A.M., Muñoz, J.A., Mediavilla, E. 2009, ApJ, 691, 1292

Mosquera, A.M., Kochanek, C.S., 2011, ApJ, 738, 96

Motta, V., Mediavilla, E., Muñoz, J.A., Falco, E., Kochanek, C.S., Arribas, S., García-Lorenzo, B., Oscoz, A., Serra-Ricart, M. 2002, ApJ, 574, 719

Moustakas, L.A., Metcalf, R.B. 2003, MNRAS, 339, 607

Muñoz, J. A., Falco, E. E., Kochanek, C. S., McLeod, B. A., & Mediavilla, E. 2004, ApJ, 605, 614

Muñoz, J. A., Mediavilla, E., Kochanek, C. S., Falco, E. E., & Mosquera, A. M. 2011, ApJ, 742, 67

Nadeau, D., Racine, R., Doyon, R., Arboit, G. 1999, ApJ, 527, 46

Nemiroff, R.J. 1988, ApJ, 335, 593

Ofek, E. O., and Maoz, D. 2003, ApJ, 594, 101

Oguri, M., Schrabback, T., Jullo, E., Ota, N., Kochanek, C. S., Dai, X., Ofek, E. O., Richards, G. T., Blandford, R. D., Falco, E. E., Fohlmeister, J. 2012. The Hidden Fortress: Structure and substructure of the complex strong lensing cluster SDSS J1029+2623. ArXiv e-prints arXiv:1209.0458.

Oguri, M., Ofek, E.O., Inada, N., Morokuma, T., Falco, E.E., Kochanek, C.S., Kayo, I., Broadhurst, T., Richards, G.T. 2008 ApJ, 676, L1

Oguri, M, Inada, N., Keeton, C.R., Pindor, B., Hennawi, J.F., Gregg, M.D., Becker, R.H., Chiu, K., Zheng, W., Ichikawa, S.-I., Suto, Y., Turner, E.L., Annis, J., Bahcall, N.A., Brinkmann, J., Castander, F.J., Eisenstein, D.J., Frieman, J.A., Goto, T., Gunn, J.E., Johnston, D.E., Kent, S.M., Nichol, R.C., Richards, G.T., Rix, H.-W., Schneider, D.P., Sheldon, E.S., Szalay, A.S. 2004 ApJ, 605, 78

Oscoz, A., Alcalde, D., Serra-Ricart, M., Mediavilla, E., Abajas, C., Barrena, R., Licandro, J., Motta, V., Muñoz, J.A. 2001, ApJ, 552, 81

Oscoz, A., Alcalde, D., Serra-Ricart, M., Mediavilla, E., Muõz, J.A. 2002, ApJ, 573, L1

Ota, N., Inada, N., Oguri, M., Mitsuda, K., Richards, G.T., Suto, Y., Brandt, W.N., Castander, F.J., Fujimoto, R., Hall, P.B., Keeton, C.R., Nichol, R.C., Schneider, D.P., Eisenstein, D.E., Frieman, J.A., Turner, E.L., Minezaki, T., Yoshii, Y. 2006, ApJ, 647, 215

Ovaldsen, J. E., Teuber, J., Schild, R. E., and Stabell, R. 2003, A&A, 402, 891

Ovaldsen, J. E., Teuber, J., Stabell, R., and Evans, A. K. D. 2003, MNRAS, 345, 795

Pelt, J., Schild, R., Refsdal, S., Stabell, R. 1998, A&A, 336, 829

Peterson, B.M. 1993, PASP, 105, 247

Poindexter, S., Morgan, N., Kochanek, C.S., Falco, E.E. 2008, ApJ, 660, 644

Poindexter, S., Morgan, N., Kochanek, C.S. 2008, ApJ, 673, 34

Pooley, D., Blackburne, J. A., Rappaport, S., Schechter, P. L. 2007, ApJ, 661, 19

Pooley, D., Rappaport, S., Blackburne, J., Schechter, P. L., Schwab, J., Wambsganss, J. 2009, ApJ, 697, 1892

Popović, L.Ć., Chartas, G. 2005, MNRAS, 353, 135

Popović, L.Ć., Mediavilla, E., Muñoz, J.A. 2001, A&A, 378, 295

Remy, M., Claeskens, J.-F., Surdej, J., Hjorth, J., Refsdal, S., Wucknitz, O., Sorensen, A. N., Grundahl, F. 1998, New Astronomy, 3, 379

Refsdal, S., Stabell, R., Pelt, J., Schild, R. 2000, A&A, 360, 10

Richards, G.T., Keeton, C.R., Pindor, B., Hennawi, J.F., Hall, P.B., Turner, E.L., Inada, N., Oguri, M., Ichikawa, S.-I., Becker, R.H., Gregg, M.D., White, R.L., Wyithe, J.S.B., Schneider, D.P., Johnston, D.E., Frieman, J.A., Brinkmann, J. 2004, ApJ, 610, 679

Schechter, P.L., Wambsganss, J. 2002, ApJ, 580, 685

Schechter, P.L., Udalski, A., Szymański, M., Kubiak, M., Pietrzyński, G., Soszyński, I., Woźniak, P., Zebruń, K., Szewczyk, O., Wyrzykowski, L. 2003, ApJ, 584, 657

Gorenstein, M.V., Cohen, N.L., Shapiro, I.I., Rogers, A.E.E., Bonometti, R.J., Falco, E.E., Bartel, N., Marcaide, J.M. 1988, ApJ, 334, 42

Schild, Rudolph E.; Smith, R. Chris 1991, AJ, 101, 813

Schneider, P., Ehlers, J., & Falco, E. 1992, Springer-Verlag

Schneider, P., Wambsganss, J. 1990, A&A, 237, 42

Sluse, D., Claeskens, J.-F., Altieri, B., Cabanac, R. A., Garcet, O., Hutsemekers, D., Jean, C., Smette, A., Surdej, J., 2006, A&A, 449, 539

Sluse, D., Schmidt, R., Courbin, F., Hutsemekers, D., Meylan, G., Eigenbrod, A., Anguita, T., Agol, E., Wambsganss, J., 2011, A&A, 528, 100

Sulentic, J. W., Marziani, P., Dultzin-Hacyan, D., 2000, ARA&A, 38, 521

Vanden Berk, D.E., Wilhite, B.C., Kron, R.G., Anderson, S.F., Brunner, R.J., Hall, P.B., Ivezić, Z., Richards, G.T., Schneider, D.P., York, D.G., Brinkmann, J.V., Lamb, D.Q., Nichol, R.C., Schlegel, D.J. 2004, ApJ, 601, 692

Vanderriest, C. 1990, LNP, 360, 210

Vanderriest, C. 1993, ASPC, 37, 338

Wambsganss, J., Paczyński, B. 1991, AJ, 102, 864

Wambsganss, J. 2006, 33rd Saas-Fee Course, p. 457

Wambsganss, J., Schmidt, R.W., Colley, W., Kundić, T., Turner, E.L. 2000, A&A, 362, L37

Walsh, D., Carswell, R.F., & Weymann, R.J. 1979, Nature, 279, 381

Wills, B.J., Wills, D. 1980, ApJ, 238, 1

Wisotzki, L., Koehler, T., Kayser, R., Reimers, D. 1993, A&A, 278, L15

Wisotzki, L., Koehler, T., Ikonomou, M., Reimers, D. 1995, A&A, 279, L59

Wisotzki, L., Becker, T., Christensen, L., Helms, A., Jahnke, K., Kelz, A., Roth, M.M., Sanchez, S.F. 2003, A&A, 408, 455

Witt, H.J., Mao, S., Schechter, P.L. 1995, ApJ, 443, 18

Woźniak, P.R., Udalski, A., Szymański, M., Kubiak, M., Pietrzyński, G., Soszyński, I., Zebruń, K. 2000, ApJ, 540, 65

Wucknitz, O., Wisotzki, L., Lopez, S., Gregg, M.D. 2003, A&A, 405, 445

Yonehara, A., Hirashita, H., Richter, P. 2008, ApJ, 478, 95